

## Supporting Information

for *Adv. Sci.*, DOI 10.1002/adv.202303682

Charge Self-Regulation of Metallic Heterostructure Ni<sub>2</sub>P@Co<sub>9</sub>S<sub>8</sub> for Alkaline Water Electrolysis with Ultralow Overpotential at Large Current Density

*Xingxing Zhu, Xue Yao, Xingyou Lang, Jie Liu, Chandra-Veer Singh\*, Erhong Song\*, Yongfu Zhu\* and Qing Jiang\**

# Supporting Information

*for*

## **Charge Self-regulation of Metallic Heterostructure Ni<sub>2</sub>P@Co<sub>9</sub>S<sub>8</sub> for Alkaline Water Electrolysis with Ultralow Overpotential at Large Current Density**

*Xingxing Zhu<sup>#</sup>, Xue Yao<sup>#</sup>, Xingyou Lang, Jie Liu, Chandra-Veer Singh\*, Erhong Song\*, Yongfu Zhu\*, Qing Jiang\**

X. Zhu, Prof. X. Lang, Prof. Y. Zhu, Prof. Q. Jiang

Key Laboratory of Automobile Materials, Ministry of Education, School of Materials Science and Engineering, Jilin University, Changchun 130022, China

E-mail: yfzhu@jlu.edu.cn

E-mail: jiangq@jlu.edu.cn

Prof. J. Liu, Prof. E. Song

State Key Lab of High Performance Ceramics and Superfine Microstructure, Shanghai Institute of Ceramics, Chinese Academy of Sciences, Shanghai, 200050, China

Prof. E. Song

Center of Materials Science and Optoelectronics Engineering, University of Chinese Academy of Sciences, Beijing, 100049, China

E-mail: ehsong@mail.sic.ac.cn;

Dr. X. Yao, Prof. C.-V. Singh

Department of Materials Science and Engineering, University of Toronto, Toronto, ON M5S 3E4, Canada

Email: [chandraveer.singh@utoronto.ca](mailto:chandraveer.singh@utoronto.ca)

Prof. C.-V. Singh

Department of Mechanical and Industrial Engineering, University of Toronto, Toronto,

ON M5S 3G8, Canada

#These authors contributed equally

\*Corresponding authors

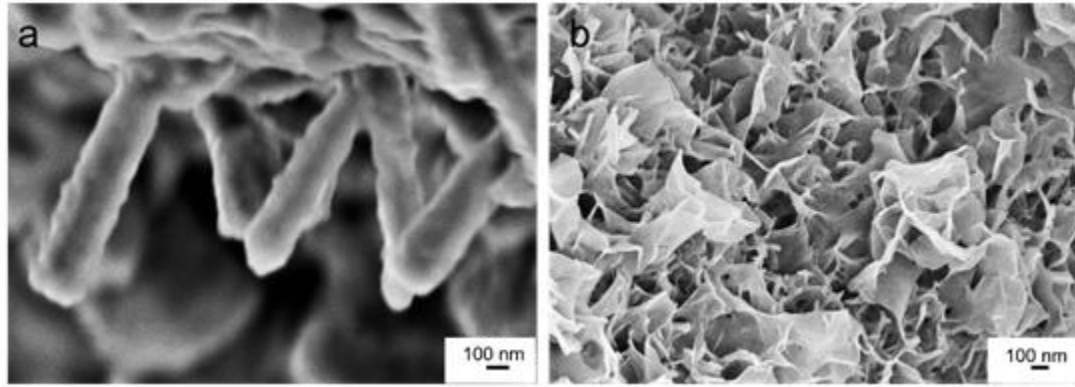


**Figure S1** FESEM observation of (a) Ni<sub>2</sub>P and (b) Co<sub>9</sub>S<sub>8</sub>.

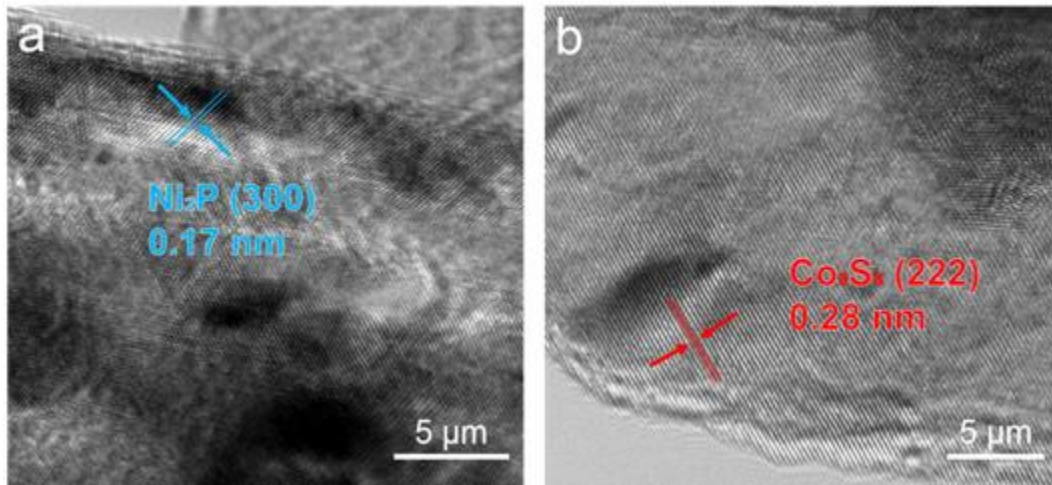


**Figure S2** HR-TEM observation of (a) Ni<sub>2</sub>P and (b) Co<sub>9</sub>S<sub>8</sub>.

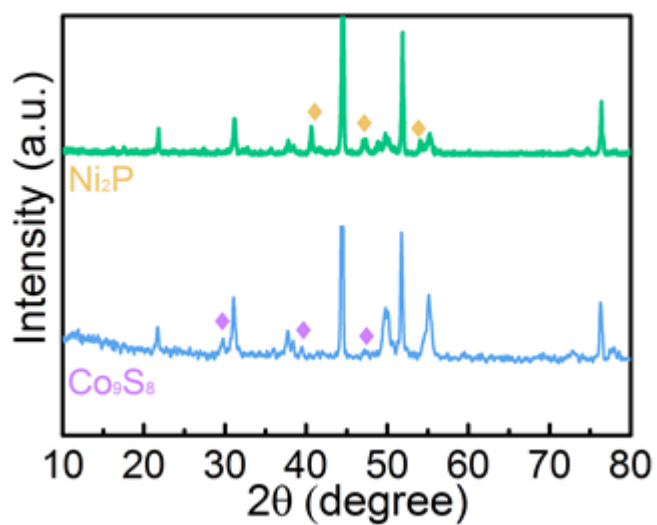


**Figure S3** XRD patterns of Ni<sub>2</sub>P and Co<sub>9</sub>S<sub>8</sub>.

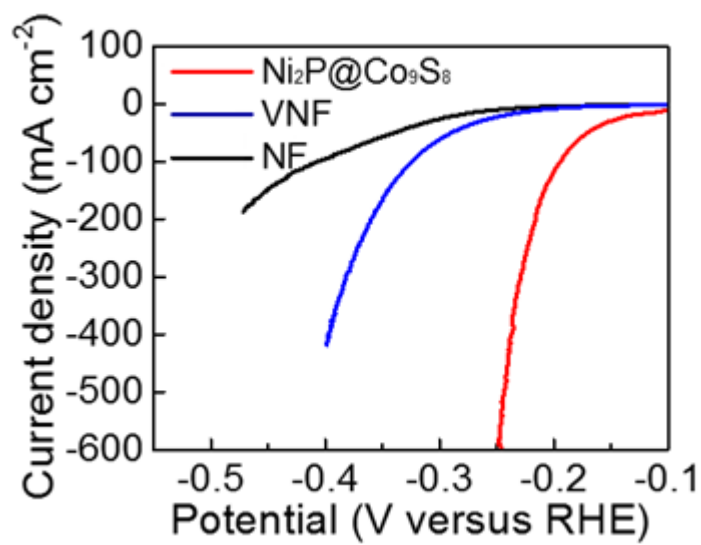


**Figure S4** LSV curves of Ni<sub>2</sub>P@Co<sub>9</sub>S<sub>8</sub>, VNF and NF for HER.

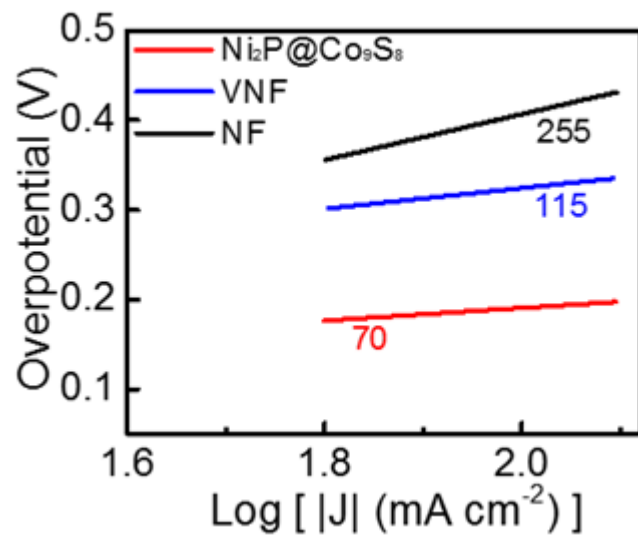


**Figure S5** Tafel slopes of Ni<sub>2</sub>P@Co<sub>9</sub>S<sub>8</sub>, VNF and NF for HER.

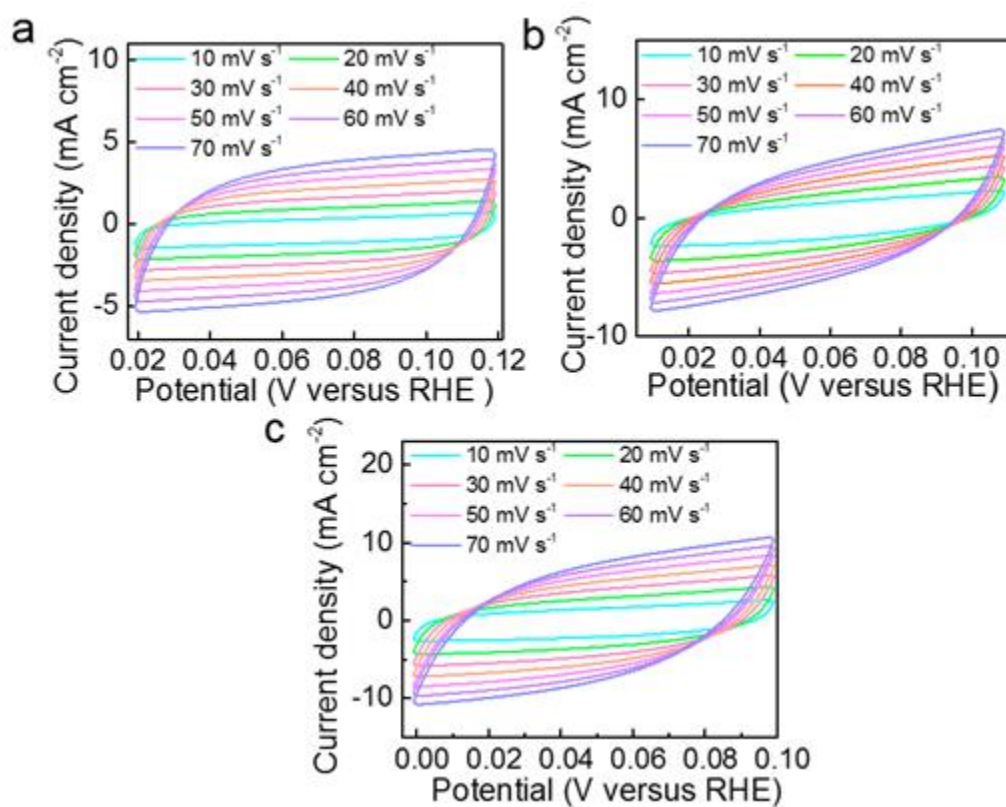


**Figure S6** CV curves of (a) Ni<sub>2</sub>P, (b) Co<sub>9</sub>S<sub>8</sub> and (c) Ni<sub>2</sub>P@Co<sub>9</sub>S<sub>8</sub> for HER.

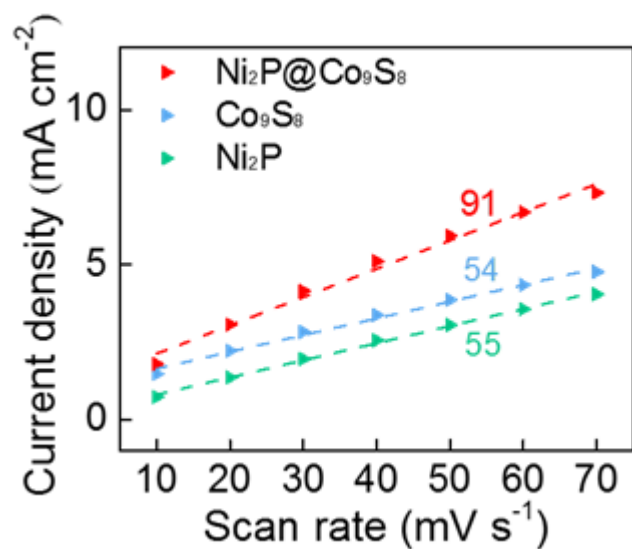


**Figure S7** Plots used to evaluate the double-layer capacitances of Ni<sub>2</sub>P, Co<sub>9</sub>S<sub>8</sub> and Ni<sub>2</sub>P@Co<sub>9</sub>S<sub>8</sub> for HER.

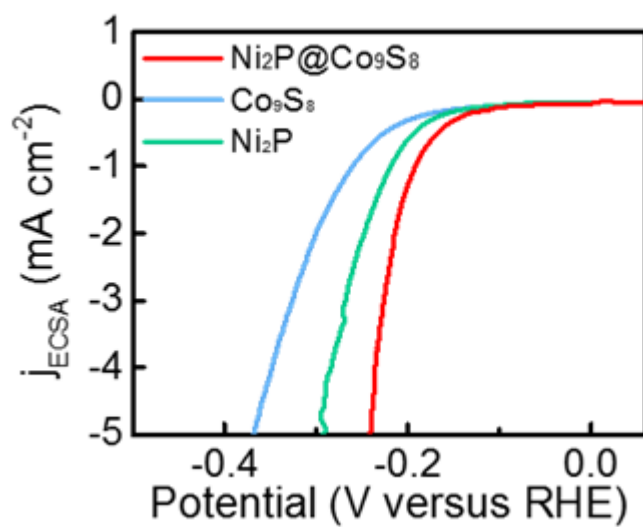


**Figure S8** Polarization curves with the current density normalized to ECSA of Ni<sub>2</sub>P, Co<sub>9</sub>S<sub>8</sub> and Ni<sub>2</sub>P@Co<sub>9</sub>S<sub>8</sub> for HER.

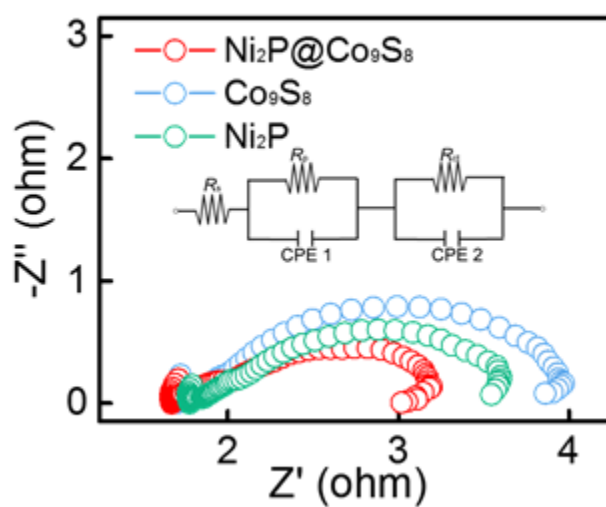


**Figure S9** Nyquist plots of Ni<sub>2</sub>P, Co<sub>9</sub>S<sub>8</sub> and Ni<sub>2</sub>P@Co<sub>9</sub>S<sub>8</sub> for HER.

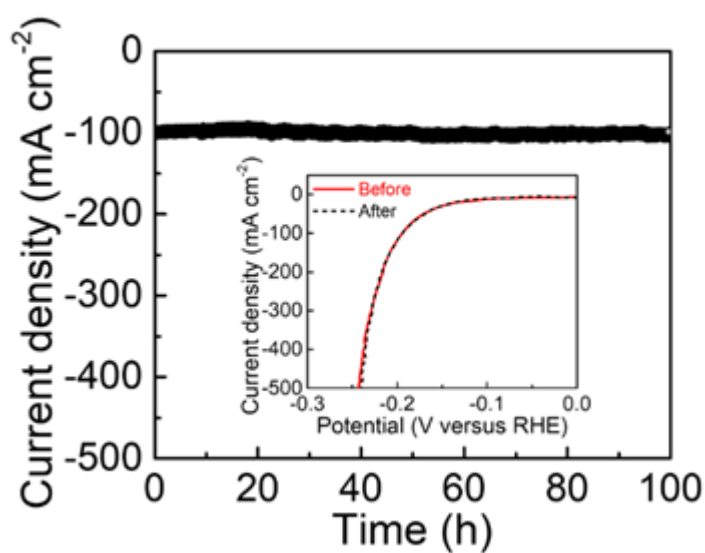


**Figure S10** The long-time current density vs time curve (*i-t* curve) of Ni<sub>2</sub>P@Co<sub>9</sub>S<sub>8</sub> at the potential of -0.188 V versus RHE, and the inset shows the polarization data for Ni<sub>2</sub>P@Co<sub>9</sub>S<sub>8</sub> before and after 100 h.



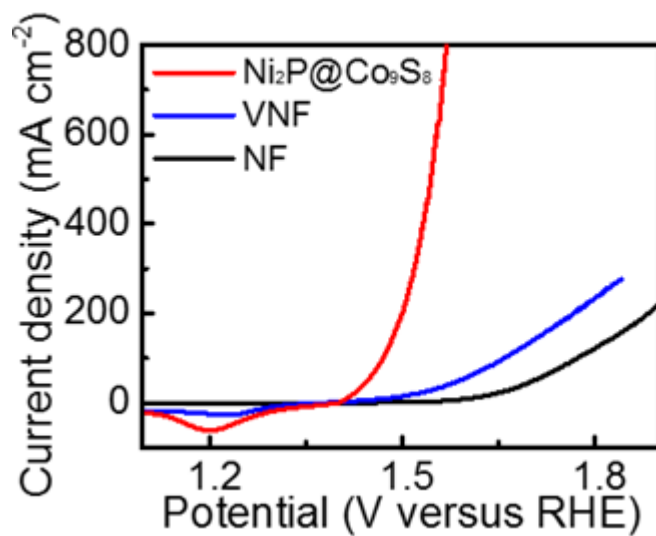


**Figure S11** Polarization curves of  $\text{Ni}_2\text{P}@Co_9S_8$ , VNF and NF for OER.

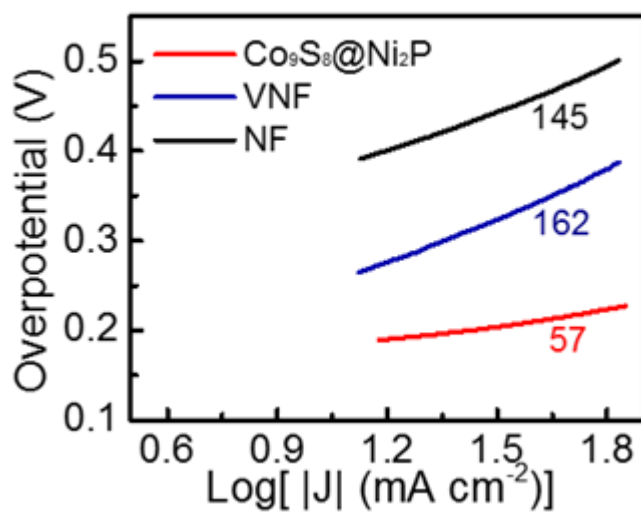


**Figure S12** Tafel slopes of  $\text{Ni}_2\text{P}@Co_9S_8$ , VNF and NF for OER.

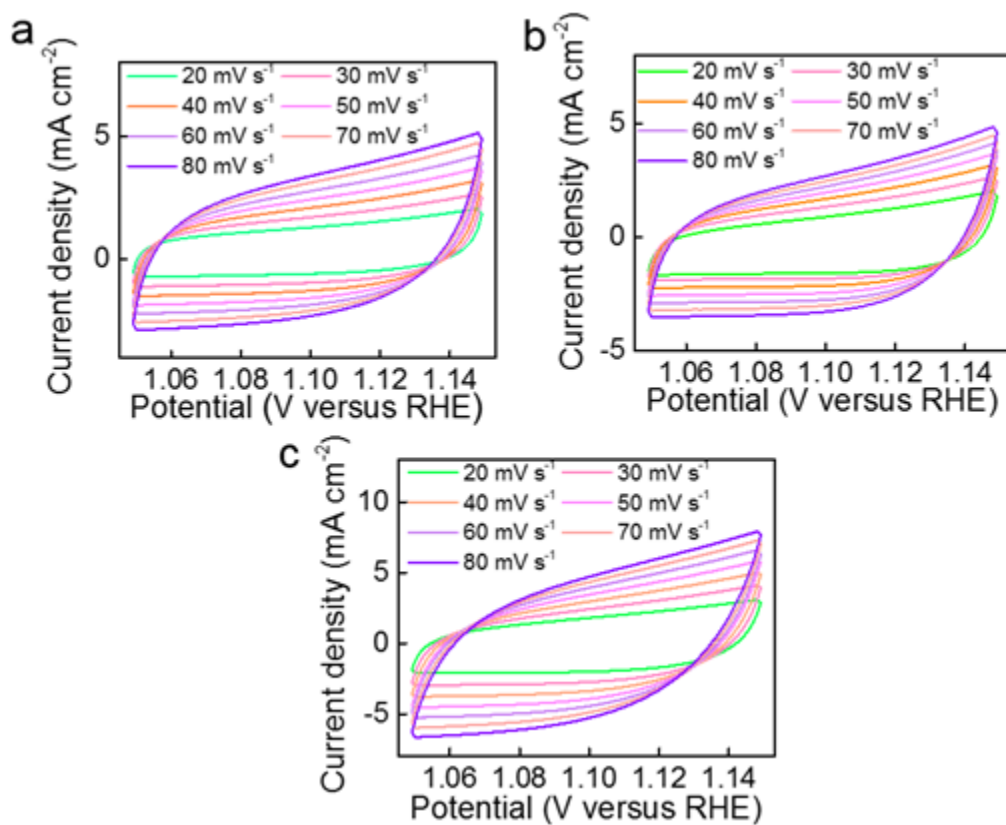


**Figure S13** CV curves of (a) Ni<sub>2</sub>P, (b) Co<sub>9</sub>S<sub>8</sub> and (c) Ni<sub>2</sub>P@Co<sub>9</sub>S<sub>8</sub> for OER.

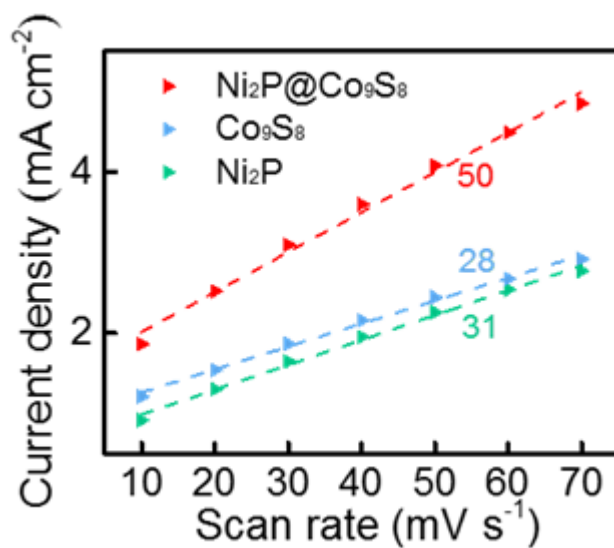


**Figure S14** Plots used to evaluate the double-layer capacitances of Ni<sub>2</sub>P, Co<sub>9</sub>S<sub>8</sub> and Ni<sub>2</sub>P@Co<sub>9</sub>S<sub>8</sub> for OER.

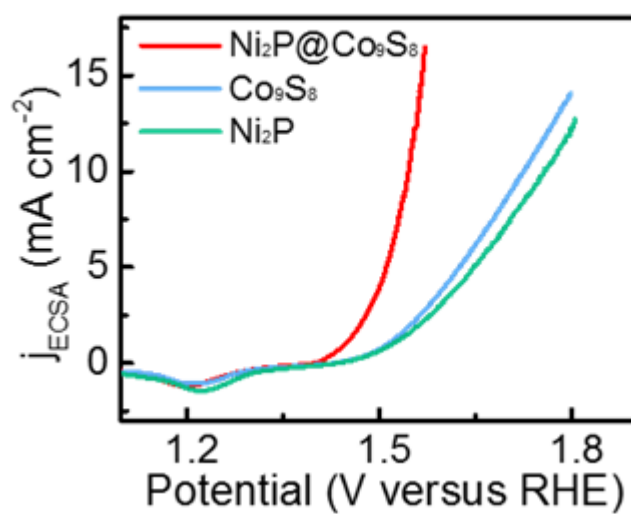


**Figure S15** Polarization curves with the current density normalized to ECSA of Ni<sub>2</sub>P, Co<sub>9</sub>S<sub>8</sub> and Ni<sub>2</sub>P@Co<sub>9</sub>S<sub>8</sub> for OER.

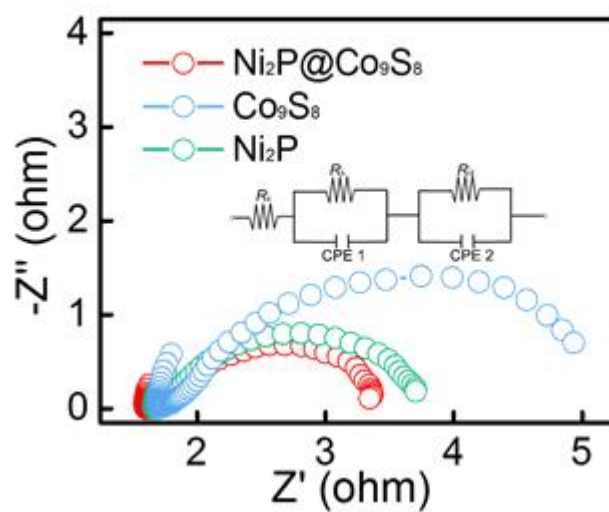


**Figure S16** Nyquist plots of Ni<sub>2</sub>P, Co<sub>9</sub>S<sub>8</sub> and Ni<sub>2</sub>P@Co<sub>9</sub>S<sub>8</sub> for OER.

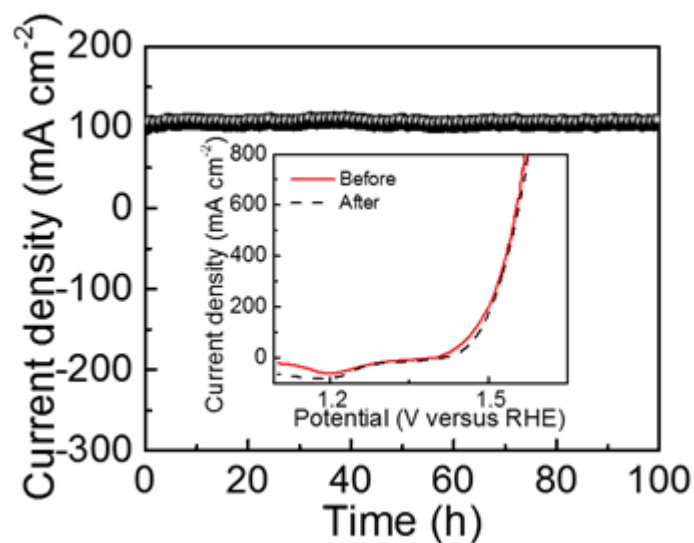


**Figure S17** The  $i$ - $t$  curve of  $\text{Ni}_2\text{P}@Co_9\text{S}_8$  at the potential of 1.485 V versus RHE, and the inset shows the polarization data for  $\text{Ni}_2\text{P}@Co_9\text{S}_8$  before and after 100 h.

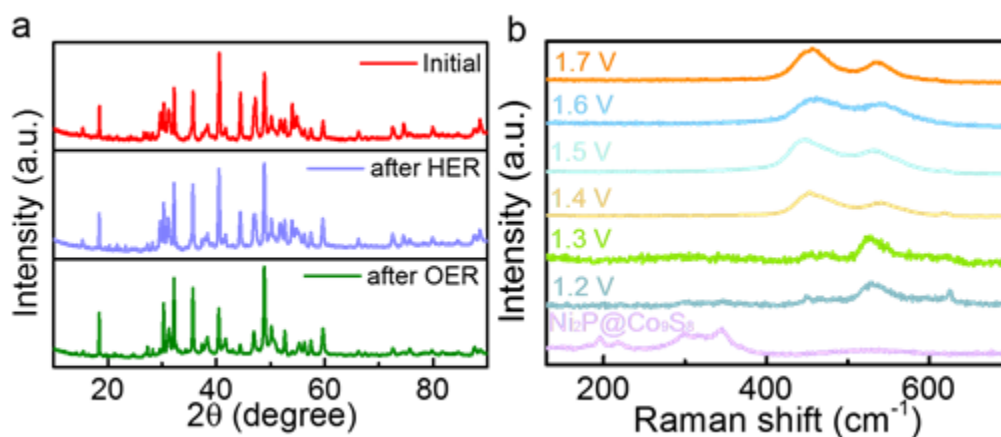


**Figure S18** (a) XRD patterns of  $\text{Ni}_2\text{P}@Co_9\text{S}_8$  before and after HER and OER reactions; (b) In situ Raman spectra of OER on  $\text{Ni}_2\text{P}@Co_9\text{S}_8$  in 1 M KOH.

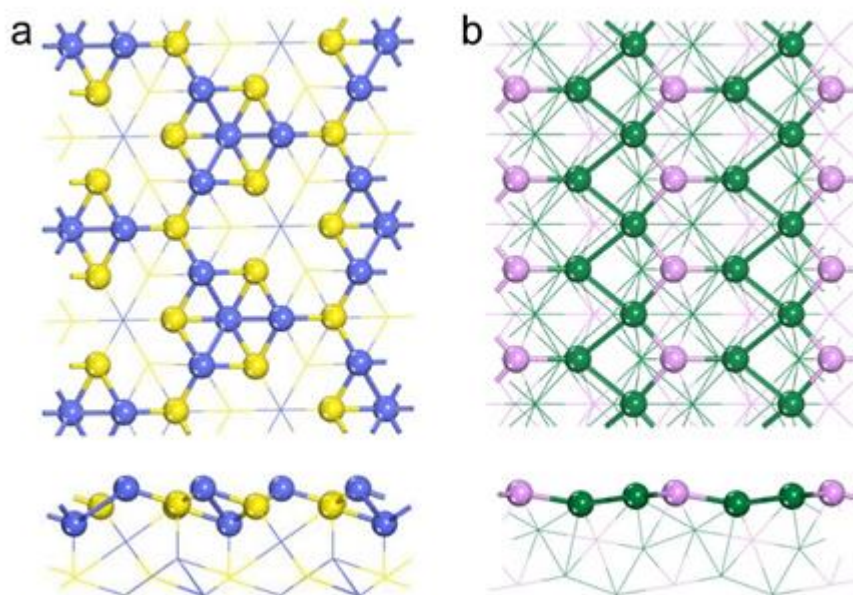


**Figure S19** Optimized structures of (a) Co<sub>9</sub>S<sub>8</sub>(111) and (b) Ni<sub>2</sub>P(100). The top layers are displayed in the ball-stick style while others are in the line style.

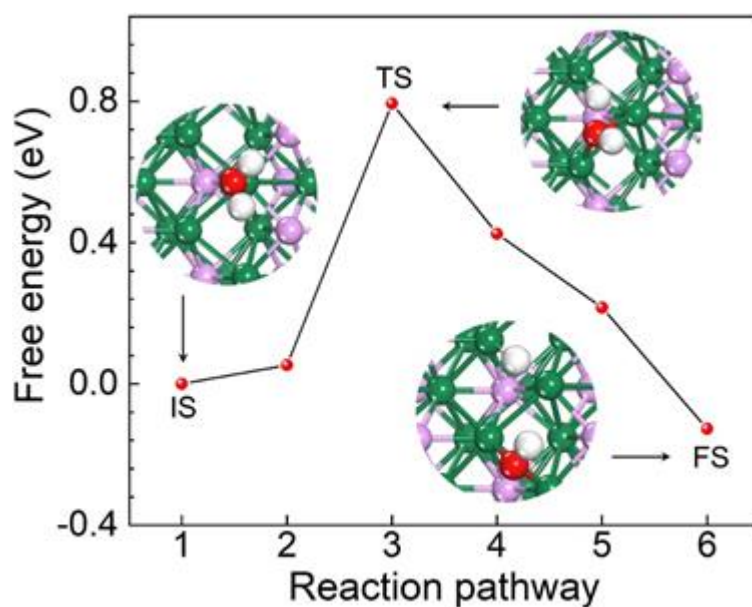


**Figure S20** The energy barrier and reaction pathway of water dissociation on Ni<sub>2</sub>P, including the corresponding configurations of IS, TS and FS.

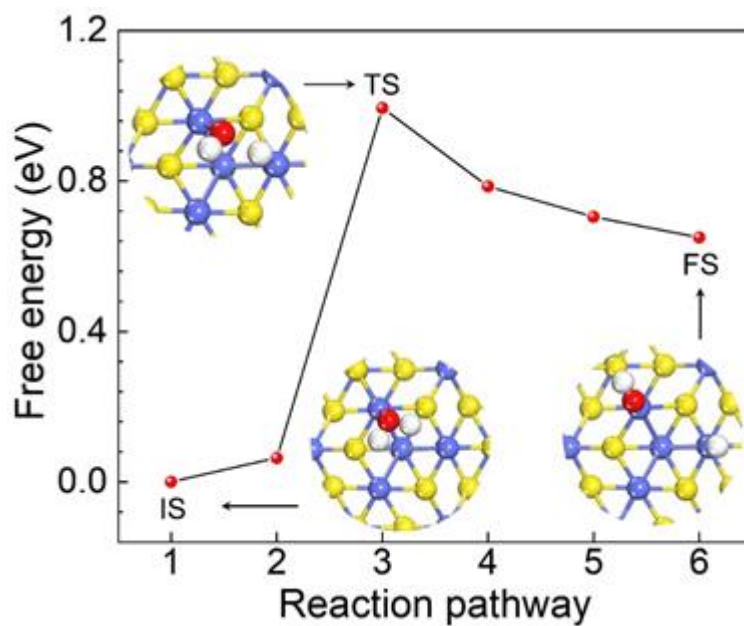


**Figure S21** The energy barrier and reaction pathway of water dissociation on  $\text{Co}_9\text{S}_8$ , including the corresponding configurations of IS, TS and FS.

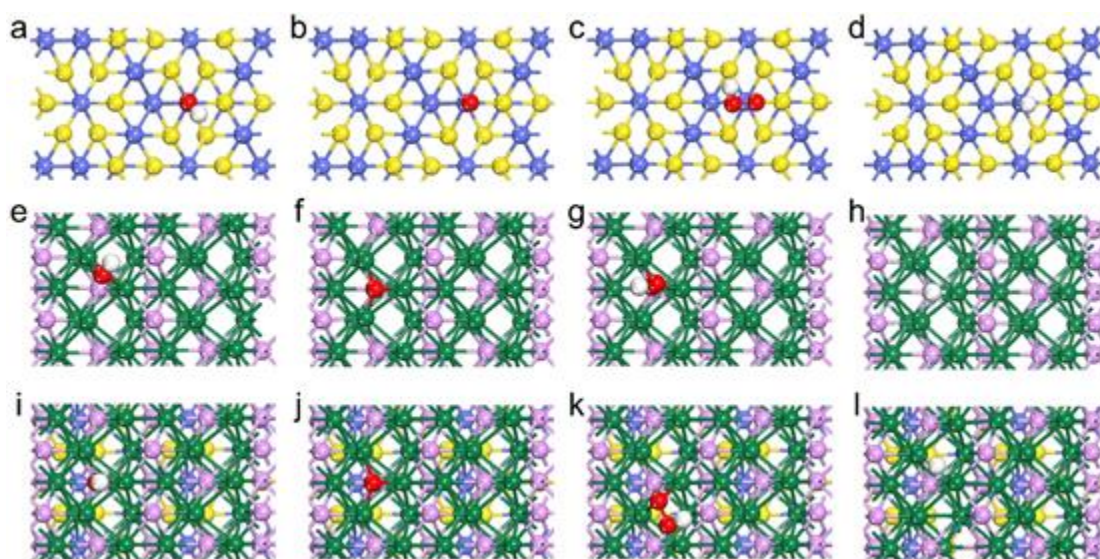


**Figure S22** Top views of  $\ast\text{OH}$ ,  $\ast\text{O}$ ,  $\ast\text{OOH}$  and  $\ast\text{H}$  on (a-d)  $\text{Co}_9\text{S}_8$ , (e-h)  $\text{Ni}_2\text{P}$  and (i-l)  $\text{Ni}_2\text{P}@ \text{Co}_9\text{S}_8$ .



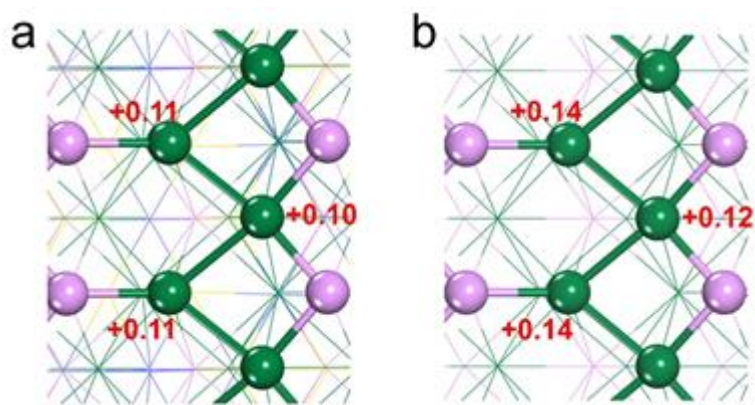


**Figure S23** Bader charge analyses of (a)  $\text{Ni}_2\text{P}@\text{Co}_9\text{S}_8$  and (b)  $\text{Ni}_2\text{P}$  including the Bader charge values of surface active Ni sites.

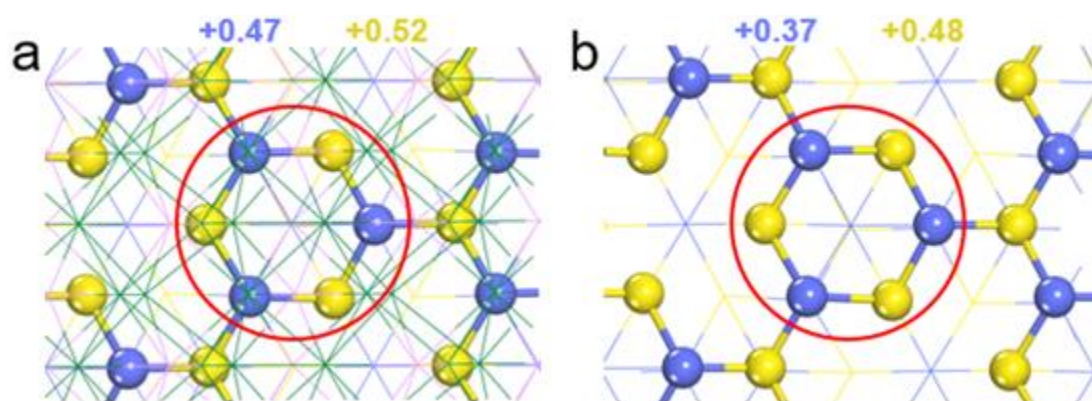


**Figure S24** Bader charge analysis of topmost Co and S atoms in (a)  $\text{Ni}_2\text{P}@\text{Co}_9\text{S}_8$  and (b)  $\text{Co}_9\text{S}_8$ . Target Co and S atoms are shown by red circles, and blue and yellow numbers are the average Bader charge values of three target Co and S atoms, respectively.

**Table S1** Calculated double layer capacitance and corresponding RF values (HER).

Catalyst	$C_{dl}$ (mF cm <sup>-2</sup> )	RF
Ni <sub>2</sub> P@Co <sub>9</sub> S <sub>8</sub>	91	2275
Co <sub>9</sub> S <sub>8</sub>	54	1350
Ni <sub>2</sub> P	55	1375

**Table S2**  $R_{ct}$  values of Ni<sub>2</sub>P@Co<sub>9</sub>S<sub>8</sub>, Co<sub>9</sub>S<sub>8</sub> and Ni<sub>2</sub>P for HER.

Catalyst	$R_{ct}$ ( $\Omega$ )
Ni <sub>2</sub> P@Co <sub>9</sub> S <sub>8</sub>	2.79
Co <sub>9</sub> S <sub>8</sub>	3.52
Ni <sub>2</sub> P	3.85

**Table S3** Calculated double layer capacitance and corresponding RF values (OER).

Catalyst	$C_{dl}$ (mF cm <sup>-2</sup> )	RF
Ni <sub>2</sub> P@Co <sub>9</sub> S <sub>8</sub>	50	1250
Co <sub>9</sub> S <sub>8</sub>	28	700
Ni <sub>2</sub> P	31	775

**Table S4**  $R_{ct}$  values of Ni<sub>2</sub>P@Co<sub>9</sub>S<sub>8</sub>, Co<sub>9</sub>S<sub>8</sub> and Ni<sub>2</sub>P for OER.

Catalyst	$R_{ct}$ ( $\Omega$ )
Ni <sub>2</sub> P@Co <sub>9</sub> S <sub>8</sub>	2.51
Co <sub>9</sub> S <sub>8</sub>	3.06
Ni <sub>2</sub> P	2.76



**Table S5** Comparison of overpotentials at 100 mA cm<sup>-2</sup> and Tafel slopes of different heterogeneous electrocatalysts recently reported for HER in 1.0 M KOH solution

Catalyst	Tafel (mV dec <sup>-1</sup> )	$\eta$ (mV) @ 100 mA cm <sup>-2</sup>	Reference
Ni <sub>2</sub> P@Co <sub>9</sub> S <sub>8</sub>	70	188	This work
c-NiP <sub>2</sub> /m-NiP <sub>2</sub>	67	200	<i>Angew. Chem. Int. Ed.</i> <b>2021</b> , 60, 259
Ni <sub>2</sub> P/MoS <sub>2</sub>	60.2	260	<i>Adv. Funct. Mater.</i> <b>2019</b> , 29, 1809151
ZnP@Ni <sub>2</sub> P-NiSe <sub>2</sub>	82	214	<i>Adv. Funct. Mater.</i> <b>2022</b> , 32, 2113224
Ni <sub>5</sub> P <sub>4</sub> -Ni <sub>2</sub> P NS	79.1	200	<i>Angew. Chem. Int. Ed.</i> <b>2015</b> , 54, 8188-8192
1T <sub>0.81</sub> -MoS <sub>2</sub> @Ni <sub>2</sub> P	79	292	<i>Nat. Commun.</i> <b>2021</b> , 12, 5260
NiCu@C	95	247	<i>J. Am. Chem. Soc.</i> <b>2018</b> , 140, 610-617
Ni <sub>5</sub> Co <sub>3</sub> Mo-OH	59	250	<i>ACS Energy Lett.</i> <b>2019</b> , 4, 952-959
Ni -ZIF/NiB	101	280	<i>Adv. Energy Mater.</i> <b>2020</b> , 10, 1902714
Mo-Co <sub>9</sub> S <sub>8</sub> @C	68	320	<i>Adv. Energy Mater.</i> <b>2020</b> , 10, 1903137
PBA@Co(OH) <sub>2</sub>	100	260	<i>Adv. Energy Mater.</i> <b>2019</b> , 9, 1802939
NiFeSe	49	230	<i>Adv. Energy Mater.</i> <b>2019</b> , 9, 1802983
Ni-Mo-N/CFC	70	250	<i>Nat. Commun.</i> <b>2019</b> , 10, 5335
Co-Ni <sub>3</sub> N/CC	185	~256	<i>Adv. Mater.</i> <b>2018</b> , 30, e1705516
FeNiP-NPHC	102	182	<i>Adv. Funct. Mater.</i> <b>2022</b> , 32, 2205767
Co <sub>0.42</sub> Fe <sub>0.58</sub> P@C	66.6	181(10)	<i>Adv. Energy Mater.</i> <b>2022</b> , 12, 2202394

**Table S6** Comparison of overpotentials at 100 mA cm<sup>-2</sup> and Tafel slopes of different heterogeneous electrocatalysts recently reported for OER in 1.0 M KOH solution

Catalyst	Tafel (mV dec <sup>-1</sup> )	$\eta$ (mV) @ 100 mA cm <sup>-2</sup>	Reference
Ni <sub>2</sub> P@Co <sub>9</sub> S <sub>8</sub>	57	253	This work
MoS <sub>2</sub> /Co <sub>9</sub> S <sub>8</sub> /Ni <sub>3</sub> S <sub>2</sub> /Ni	58	420	<i>J. Am. Chem. Soc.</i> <b>2019</b> , <i>141</i> , 10417-10430
Co <sub>3</sub> O <sub>4</sub> -NP/N-rGO	62	380	<i>Adv. Energy Mater.</i> <b>2018</b> <i>8</i> , 1702222
CoFe <sub>2</sub> O <sub>4</sub> @N-CNFs	80	349	<i>Adv. Sci.</i> <b>2017</b> , <i>4</i> , 1700226
CF/VGSs/MoS	113	450	<i>Nat. Commun.</i> <b>2021</b> , <i>12</i> , 1380
Co-MoS <sub>2</sub> /BCCF-21	85	370	<i>Adv. Mater.</i> <b>2018</b> , <i>30</i> , 1801450
Ni <sub>2</sub> P-NiSe <sub>2</sub>	71	326	<i>Adv. Funct. Mater.</i> <b>2022</b> , <i>32</i> , 2113224
Fe-Ni <sub>2</sub> P@Cu <sub>x</sub> S	59	390	<i>ACS Energy Lett.</i> <b>2019</b> , <i>4</i> , 952-959
S-(Ni,Fe)OOH	48.9	281	<i>Energy Environ. Sci.</i> <b>2020</b> , <i>13</i> , 3439-3446
W <sub>0.5</sub> Co <sub>0.4</sub> Fe <sub>0.1</sub> /NF	310	42	<i>Angew. Chem. Int. Ed.</i> <b>2017</b> , <i>56</i> , 4502-4506
2D/1D FeNi LDH/MOF	37.1	272	<i>Adv. Funct. Mater.</i> <b>2021</b> , <i>31</i> , 2103318
Fe <sub>2</sub> Ni-BPTC/CC	42	365	<i>Angew. Chem. Int. Ed.</i> <b>2018</b> , <i>57</i> , 9660
(CrMnFeCoNi) <sub>S<sub>x</sub></sub>	66	295	<i>Adv. Energy Mater.</i> <b>2021</b> , <i>11</i> , 2002887
CoMoNiS-NF-31	53	260	<i>J. Am. Chem. Soc.</i> <b>2019</b> , <i>141</i> , 10417-10430.
MoO <sub>x</sub> /Ni <sub>3</sub> S <sub>2</sub>	72	310	<i>Adv. Funct. Mater.</i> <b>2016</b> , <i>26</i> , 4839.
(Fe,Co)OOH/MI	73	290	<i>Adv. Mater.</i> <b>2022</b> , <i>34</i> , 2200270
CoNiFeCu	43.5	292	<i>Adv. Mater.</i> <b>2022</b> , <i>34</i> , 2109108
MoS <sub>2</sub> /NiFe LDH  MoNiFe	23	290	<i>Nat. Commun.</i> <b>2022</b> , <i>13</i> , 2191

CoNiRu-NT	67	335	<i>Adv. Mater.</i> <b>2022</b> , <i>34</i> , 2107488
FeCoNiMnRu/CNF	61.3	308	<i>Nat. Commun.</i> <b>2022</b> , <i>13</i> , 2662
Mn-NG	55	337(10)	<i>Nat. Catal.</i> <b>2018</b> , <i>1</i> , 870-877
Ni-NHGF	61	331(10)	<i>Nat. Catal.</i> <b>2018</b> , <i>1</i> , 63-72

**Table S7** Comparison of cell voltages at 10 and 100 mA cm<sup>-2</sup> and stabilities of different bifunctional non-noble metal electrocatalysts recently reported for overall water splitting in 1.0 M KOH solution

Catalyst	Cell voltage at 10 mA cm <sup>-2</sup> (V)	Cell voltage at 100 mA cm <sup>-2</sup> (V)	Reference
Ni <sub>2</sub> P@Co <sub>9</sub> S <sub>8</sub>	1.46	1.66	This work
FeCoNi/CC	1.55	2.00	<i>Adv. Energy Mater.</i> <b>2019</b> , <i>9</i> , 1901312
Co <sub>3</sub> S <sub>4</sub> /MOF	1.55	1.90	<i>Adv. Mater.</i> <b>2019</b> , <i>31</i> , 1806672
Ni/γ-Fe <sub>2</sub> O <sub>3</sub>	1.47	1.77	<i>Nat. Commun.</i> <b>2019</b> , <i>10</i> , 5599
CoFeZrO <sub>x</sub>	1.63	1.78	<i>Adv. Mater.</i> <b>2019</b> , <i>31</i> , 1901439
Ni-ZIF/NiB	1.54	1.77	<i>Adv. Energy Mater.</i> <b>2020</b> , <i>10</i> , 1902714
PBA@Co(OH) <sub>2</sub>	1.65	1.99	<i>Adv. Energy Mater.</i> <b>2019</b> , <i>9</i> , 1802939
Cr/FeNi-P	1.54	1.70	<i>Adv. Mater.</i> <b>2019</b> , <i>31</i> , 1900178
CoMoNiS	1.54	2.09	<i>J. Am. Chem. Soc.</i> <b>2019</b> , <i>141</i> , 10417-10430
Au/Ni <sub>3</sub> S <sub>2</sub> /NF	1.52	1.82*	<i>Appl. Catal. B: Environ.</i> <b>2022</b> , <i>304</i> , 120935
MH-TMO	1.49	1.72	<i>Adv. Energy Mater.</i> <b>2022</b> , <i>12</i> , 2200067
BPIr-be	1.57	1.78	<i>Adv. Mater.</i> <b>2021</b> , <i>33</i> , 2104638
O-CMMOFs-NF	1.47	1.85	<i>Appl. Catal. B: Environ.</i> <b>2022</b> , <i>307</i> , 121151
Ni-MoO <sub>2</sub> /NF-IH	1.50	1.72	<i>Adv. Funct. Mater.</i> <b>2021</b> , <i>31</i> , 2009580.
CoFeO@BP	1.58	1.78	<i>Angew. Chem. Int. Ed.</i> <b>2020</b> , <i>59</i> , 21106.
MoS <sub>2</sub> /NiFe LDH  MoNiFe	1.61	1.73	<i>Nat. Commun.</i> <b>2022</b> , <i>13</i> , 2191

---

CoFeP@C	1.55	1.78	<i>Adv. Energy Mater.</i> <b>2022</b> , 12, 2202394
FeCoNi MOF	1.60	1.90	<i>J. Am. Chem. Soc.</i> <b>2022</b> , 144, 3411

---

**Table S8** Comparison of the overpotentials at 200 mA cm<sup>-2</sup> toward the HER in 1 M KOH of the Ni<sub>2</sub>P@Co<sub>9</sub>S<sub>8</sub> with other reported high-performance bifunctional catalysts.

Catalyst	$\eta$ (mV) @ 200 mA cm <sup>-2</sup>	Reference
Ni <sub>2</sub> P@Co <sub>9</sub> S <sub>8</sub>	204	This work
CoNC@Co <sub>2</sub> N/CPs	330	<i>Adv. Energy Mater.</i> <b>2020</b> , <i>10</i> , 2002214
Ni-N <sub>3</sub>	345	<i>Adv. Mater.</i> <b>2020</b> , <i>33</i> , 2003846
Cu <sub>1</sub> Ni <sub>2</sub> -N	255	<i>Adv. Energy Mater.</i> <b>2019</b> , <i>9</i> , 1900390
Ni <sub>5</sub> Co <sub>3</sub> Mo-OH	290	<i>ACS Energy Lett.</i> <b>2019</b> , <i>4</i> , 952-959
Cu <sub>3</sub> N	335	<i>ACS Energy Lett.</i> <b>2019</b> , <i>4</i> , 747-754
NiMoN/CFC	400	<i>Nat. Commun.</i> <b>2019</b> , <i>10</i> , 5335
FeNiS/Ni	300	<i>Adv. Energy Mater.</i> <b>2020</b> , 2001963
NiFeP/graphene	290	<i>Adv. Mater.</i> <b>2020</b> , <i>32</i> , 1908201
NiFeSe	325	<i>Adv. Energy Mater.</i> <b>2019</b> , <i>9</i> , 1802983

**Table S9** Comparison of the overpotentials at 200 mA cm<sup>-2</sup> toward the OER in 1 M KOH of the Ni<sub>2</sub>P@Co<sub>9</sub>S<sub>8</sub> with other reported high-performance bifunctional catalysts.

Catalyst	$\eta$ (mV) @ 200 mA cm <sup>-2</sup>	Reference
Ni <sub>2</sub> P@Co <sub>9</sub> S <sub>8</sub>	276	This work
NiCo LDH/NiCoS	378	<i>Nano Res.</i> <b>2022</b> , <i>15</i> , 4986-4995
CoOOH	340	<i>J. Mater. Chem. A</i> <b>2019</b> , <i>7</i> , 7777-7783
Co <sub>2</sub> P-Co <sub>3</sub> O <sub>4</sub>	405	<i>Adv. Energy Mater.</i> <b>2018</b> , <i>8</i> , 1802445
Ni/MoN/rNS)	533	<i>Adv. Sci.</i> <b>2022</b> , <i>9</i> , 2105869
Ni <sub>x</sub> Co <sub>3-x</sub> S <sub>4</sub> /Ni <sub>3</sub> S <sub>2</sub>	318	<i>Nano Energy</i> <b>2017</b> , <i>35</i> , 161-170
MoO <sub>x</sub> /Ni <sub>3</sub> S <sub>2</sub>	312	<i>Adv. Funct. Mater.</i> <b>2016</b> , <i>26</i> , 4839-4847
EG/Co <sub>0.85</sub> Se/NiFe-LDH	290*	<i>Energy Environ. Sci.</i> <b>2016</b> , <i>9</i> , 478-483
FeCoNiCuMn HEA/CNF	386	<i>Energy Environ. Sci.</i> <b>2023</b> , <i>16</i> , 619-628
MX@MOF-Co <sub>2</sub> P	407	<i>J. Mater. Sci. Technol.</i> <b>2023</b> , <i>145</i> , 74-82
Ni/MoN/rNS	533	<i>Adv. Sci.</i> <b>2022</b> , <i>9</i> , 2105869
Co/CoO/Co(OH) <sub>2</sub>	360*	<i>Appl. Catal. B</i> <b>2021</b> , <i>292</i> , 120063
Ir-1/Ni <sub>1.6</sub> Mn <sub>1.4</sub> O <sub>4</sub>	350	<i>Adv. Sci.</i> <b>2022</b> , <i>9</i> , 2200529

\*The data were calculated according to the curves given in the literature

**Table S10** Comparison of the overpotentials at 200 mA cm<sup>-2</sup> toward the overall water splitting in 1 M KOH of the Ni<sub>2</sub>P@Co<sub>9</sub>S<sub>8</sub> with other reported high-performance bifunctional catalysts

Catalyst	Cell voltage at 200 mA cm <sup>-2</sup> (V)	Reference
Ni <sub>2</sub> P@Co <sub>9</sub> S <sub>8</sub>	1.76	This work
Co <sub>3</sub> Se <sub>4</sub> /CF	2.11	<i>Adv. Energy Mater.</i> , <b>2017</b> , 7, 1602579
CoP/NCNHP	1.97	<i>J. Am. Chem. Soc.</i> <b>2018</b> , 140, 2610-2618
NiCoP@NF-100	1.87	<i>J. Energy Chem.</i> <b>2020</b> , 50, 395-401
CoPO/NF	1.98	<i>Adv. Funct. Mater.</i> <b>2018</b> , 28, 1706120
NC@CuCo <sub>2</sub> N <sub>x</sub> /CF	1.93	<i>Adv. Funct. Mater.</i> <b>2017</b> , 27, 1704169
Ni-P/NF	2.17*	<i>J. Mater. Chem. A.</i> <b>2016</b> , 4, 5639-5646
Ni-P/CP	3.3*	<i>Adv. Funct. Mater.</i> <b>2016</b> , 26, 4067-4077
Cu <sub>3</sub> N	1.8	<i>ACS Energy Lett.</i> <b>2019</b> , 4, 747-754
FeNiS/Ni	1.95	<i>Adv. Energy Mater.</i> <b>2020</b> , 2001963.
FeCoNi/CC	2.13	<i>Adv. Energy Mater.</i> <b>2019</b> , 9, 1901312.
NiFeP/graphene	1.90	<i>Adv. Mater.</i> <b>2020</b> , 32, 1908201



---

CoNC	1.91	<i>Energy Environ. Sci.</i> <b>2020</b> , <i>13</i> , 545-553
FeCo/Co <sub>2</sub> P@C	2.1	<i>Adv. Energy Mater.</i> <b>2020</b> , <i>10</i> , 1903854.
CoNSC	1.78	<i>Adv. Energy Mater.</i> <b>2020</b> , <i>10</i> , 2002896
NiCoP/NF	1.98	<i>Nano Lett.</i> <b>2016</b> , <i>16</i> , 7718- 7725

---

\*The data were calculated according to the curves given in the literature